MALAT1 enhanced the proliferation of human osteoblasts treated with ultra-high molecular weight polyethylene by targeting VEGF via miR-22-5p

XUCHENG YANG, YINGYING ZHANG, YUSHENG LI and TING WEN

Department of Orthopaedics, Xiangya Hospital Central South University, Changsha, Hunan 410008, P.R. China

Received October 25, 2016; Accepted December 8, 2017

DOI: 10.3892/ijmm.2018.3363

Abstract. Osteolysis associated with an implanted prosthesis is the major cause of failure in prosthesis implantation, and a severe public health issue worldwide. The type of bone metabolism associated with this disorder has been a major focus for improving the outcomes of patients with osteolysis. The role of metastasis-associated lung adenocarcinoma transcript 1 (MALAT1; a member of the long coding RNA family) during the onset of osteolysis and the related molecular regulatory mechanism in ultra-high molecular weight polyethylene (UHMWPE)-treated hFOB 1.19 cells were investigated in the current study. The effect of MALAT1 knockdown on cell viability, cell apoptosis and osteolysis-associated signaling were also examined, and the interactions that occurred between MALAT1 and an anti-osteolysis molecule, microRNA (miR)-22-5p were investigated. Additionally, knockdown of vascular endothelial growth factor (VEGF) exerted similar biological effects as observed following miR-22-5p overexpression. The data showed that MALAT1 and pro-osteolysis indicators, receptor activator of nuclear factor-κB ligand (RANKL) and VEGF were upregulated in clinical interface membrane samples. Knockdown of MALAT1 inhibited the growth of UHMWPE-treated hFOB 1.19 cells, and this effect was associated with the upregulation of OPG, and downregulation of RANKL and VEGF. Results of a dual luciferase assay confirmed the interaction between VEGF and miR-22-5p, and also between MALAT1 and miR-22-5p. Additionally, subsequent assays indicated that overexpression of MALAT1 suppressed the anti-osteolysis effect of miR-22-5p, which would further induce VEGF expression. The data indicated that MALAT1 has an in port ant role in the onset of osteolysis via its ability to induce RANKL expression and inhibit the effect of miR-22-5p.

Correspondence to: Professor Ting Wen, Department of Orthopaedics, Xiangya Hospital Central South University, 87 Xiangya Road, Changsha, Hunan 410008, P.R. China
E-mail: wentingdoc@sina.com

Key words: metastasis-associated lung adenocarcinoma transcript 1, vascular endothelial growth factor, receptor activator of nuclear factor-κB ligand, miR-22-5p, osteolysis

Introduction

Joint arthroplasty is an effective treatment for severe trauma and arthritic joint disorders, in that it provides reliable long-term improvements in joint function, pain and quality of life (1). However, chronic wear on these prostheses can generate metallic, polyethylene or ceramic debris, which is released into the joint space and becomes embedded into synovial tissues (2). The deposition of the debris induces inflammatory cytokine production that directly or indirectly initiates unexpected bone erosion (osteolysis) resulting from the differentiation and activation of osteoclasts (3-5). Several studies have reported that aseptic loosening due to periprosthetic osteolysis has become the major cause of failure following prosthesis implantation, and has a prevalence of >10% (6-8). Unfortunately, the only treatment currently available for periprosthetic osteolysis is revision surgery; however, this method is rendered less effective by its greater rate of morbidity and poorer functional outcomes. Given the crucial role that prosthesis implantation has in treating patients with joint disorders, it is important to identify key modulators involved in the osteolytic process if the clinical outcomes of patients receiving joint arthroplasty are to be improved. The development, remodeling and repair of bone tissue are critically dependent on angiogenesis (9). Osteoclasts and chondroclasts first appear in conjunction with blood vessel invasion. Furthermore, the formation of new capillaries and resorption of mineralized matrices are essential events for bone morphogenesis and growth (10). Therefore, cytokines that have determinant roles in the angiogenesis process also have key functions in maintaining the skeletal system. Vascular endothelial growth factor (VEGF) is the most important mediator of angiogenesis (11). VEGF is produced by various types of cells, and is expressed in osteoclasts and chondroclasts in skeletal tissue (12,13). Nakagawa *et al* (9) reported that VEGF directly increases osteoclastic bone resorption and the survival time of mature osteoclasts. Henriksen *et al* (14) reported that VEGF is capable of inducing osteoclast differentiation and the functioning of receptor activator of nuclear factor-κB ligand (RANKL). Taken together, these findings indicate that VEGF promotes the onset of osteolysis. Thus, modulation of VEGF activity may be a strategy for alleviating bone erosion following joint arthroplasty.

Mammalian cells produce various non-coding RNA molecules, including small non-coding RNAs such as microRNAs (miRs) and long non-coding RNAs (lncRNAs).

The use of miRs to regulate gene expression in treatment of various diseases has been previously reported (15). Furthermore, lncRNAs are increasingly recognized as important modulators of diverse cellular processes, including cell proliferation, cell-cycle progression, apoptosis and cell growth (16). Several miRs have been reported to inhibit the transcription of factors involved in VEGF regulation (17-19). One such miR is miR-22, which was reported to suppress VEGF activity in colon cancer (20). This infers that upregulation of miR-22 during the osteogenic differentiation of human adipose tissue-derived mesenchymal stem cells may have a promoting effect (21), which is paradoxical to its suppressive effect on VEGF activity. Thus, it is necessary to investigate the association between miR-22 and VEGF during the osteolytic process. Aside from miRs, lncRNAs also affect development of the skeletal system. Che *et al* (22) reported that metastasis-associated lung adenocarcinoma transcript 1 (MALAT1*)* knockdown reduced growth inhibition and cell cycle arrest in RANKL-induced cells. Additionally, MALAT1 is able to regulate miR-22 activity via a competitive endogenous RNA mechanism (23). Taken together, these findings suggest that MALAT1, miR-22, VEGF and RANKL all interact with each other during the osteolytic process that reduces the benefits of joint arthroplasty.

Therefore, the present study was performed to reveal the molecular regulatory mechanism of these various factors (MALAT1, miR-22, VEGF and RANKL) in an osteolysis model using hFOB 1.19 osteoblast cells. The expression levels of osteolysis-related indicators were examined in clinical interface membrane samples and synovial tissues, and MALAT1 knockdown hFOB 1.19 cells. The findings suggest that during the osteolytic process, MALAT1 increases RANKL activity and indirectly activates the VEGF pathway by suppressing miR-22-5p activity.

Materials and methods

Chemicals. Antibodies against VEGF (BA0407), osteoprotegerin (OPG), RANKL (M00363) and GAPDH (A00227) were all purchased from Wuhan Boster Biological Technology, Ltd. (Wuhan, China). Mimics (5'-AGUUCUUCAGUGGCAAGCUUUA-3'), inhibitors (5'-UAAAGCUUGCCACUGAAGAACU-3'), negative control (NC; 5'-UUCUCCGAACGUGUCACGUTT-3') miR-22-5p, specific MALAT1 small interfering RNA (siRNA), and siVEGF (5'-UUCCUCUGGUGGCCAGGGGCA-3') and scrambled NC MALAT1 siRNA (siMALAT1, 5'-AAGAAAAAUAAAAGCUUUCCU-3' and siNC, 5'-ACGUGACACGUUCGGAGAATT-3') were all obtained from Shanghai GenePharma Co., Ltd. (Shanghai, China). Fragments of the 3' untranslated region (3'UTR) of MALAT1/VEGF and the mutant 3'UTR of MALAT1/VEGF were amplified from human hFOB 1.19 cells by PCR and inserted into a psiCHECK-2 vector (vector containing firefly luciferase under control of the SV40 promoter; Promega Corporation, Madison, WI, USA) to create different wild type (WT) and mutant (MUT) versions of plasmids. The ultra-high molecular weight polyethylene (UHMWPE) particles (Clariant, Gersthofen, Germany) were utilized for establishing *in vitro* osteolysis model and the size of UHMWPE used was 0.05-11.6 μm (mean, 1.74±1.43 μm). Prior to injection, the particles were tested in a quantitative limulus amebocyte lysate assay to ensure their endotoxin level was <0.25 EU/ml. Following testing, the particles were sterilized in 99.5% ethanol at room temperature for 24 h; after which, they were dried and suspended in fetal calf serum (cat. no. 10099133; Thermo Fisher Scientific, Inc., Waltham, MA, USA).

Cell culture. Human hFOB 1.19 fetal osteoblastic cell line was obtained from Bioleaf Biotech Co., Ltd. (Shanghai, China). The cells were cultured in a 1:1 mixture of Ham's F12 medium and Dulbecco's modified Eagle's medium (Thermo Fisher Scientific, Inc.) without phenol red, but supplemented with 10% fetal bovine serum (Thermo Fisher Scientific, Inc.), 50 μg/ml penicillin, and 50 mg/l gentamicin (Sigma-Aldrich; Merck KGaA, Darmstadt, Germany) at pH 7.2 in a humidified atmosphere containing 5% CO_2.

Clinical sample collection. From January 2015 to September 2016, 8 samples of interface membrane tissue were collected from patients with prosthetic aseptic loosening at Xiangya Hospital (Changsha, China), and used to investigate the expression status of molecules involved the osteolytic process that occurred after implantation of a prosthesis (10 samples). Eight samples of synovial tissue collected from patients that received a hip operation were used as normal control samples. All enrolled patients, with 9/18 males, were provided with detailed information concerning the clinical, pathological and prognostic aspects of their disease, and were diagnosed by a micro-computed tomography scan (data not shown). The study protocol was approved by the Research Ethics Committee of the Xiangya Hospital of Central South University (Changsha, China). The Hospital's Ethics Committee approved the study-associated screening, inspection and data collection procedures, and all subjects signed a written informed consent document. Information concerning the enrolled patients is presented in Table I. All study procedures complied with provisions in the Declaration of Helsinki.

Cell seeding and particle treatment. Human hFOB 1.19 osteoblast cells ($1x10^4$ cells/well)were transferred into 96-well plates, and incubated at 37˚C in an atmosphere containing 5% CO_2. Fresh medium containing UHMWPE particles was added to each well after 24 h of culture. The inherent hydrophobicity of polyethylene was used to ensure that sufficient contact occurred between the cells and particles. The cell-particle ratio was 1:500, and the particle treatment method was previously described by Kauther *et al* (24).

Experimental design and transfection. Transfection with mimics or plasmids was performed using Lipofectamine® 2000 (Thermo Fisher Scientific, Inc., Waltham, MA, USA) according to the manufacturer's instructions. Details of the experimental designs are provided below.

The following two groups of cells (i and ii) were used in assays designed to determine how MALAT1 functions during the osteolytic process: i) NC group (UHMWPE-treated hFOB cells transfected with NC siRNA, 100 pmol per 6 well plates); and ii) siMALAT1 group (UHMWPE-treated hFOB cells transfected with specific MALAT1 siRNA, 100 pmol per 6 well plates).

Table I. Clinical features of patients involved in the study.

Patient no.	Gender	Age (years)	Diagnosis	Operation
1	Female	77	Prosthetic aseptic loosening (left hip)	Revision (left hip)
2	Female	61	Prosthetic aseptic loosening (left hip)	Revision (left hip)
3	Male	NR	Prosthetic aseptic loosening (right hip)	Revision (right hip)
4	Male	47	Prosthetic aseptic loosening (left hip)	Revision (left hip)
5	Male	66	Prosthetic aseptic loosening (right hip)	Revision (right hip)
6	Female	NR	-	-
7	Female	40	Femoral neck fracture (left)	Total hip replacement (left hip)
8	Male	86	Femoral neck fracture (left)	Total hip replacement (left hip)
9	Male	75	Femoral neck fracture (left)	Total hip replacement (left hip)
10	Female	57	Femoral neck fracture (left)	Total hip replacement (left hip)
11	Male	40	Femoral neck fracture (bilateral)	Total hip replacement (bilateral)
12	Male	48	Prosthetic aseptic loosening (left hip)	Revision (left hip)
13	Male	40	Femoral neck fracture (bilateral)	Total hip replacement (bilateral)
14	Male	68	Prosthetic aseptic loosening (right hip)	Revision (right hip)
15	Female	79	Femoral neck fracture (left)	Revision (left hip)
16	Female	69	Prosthetic aseptic loosening (right hip)	Revision (right hip)
17	Female	67	Femoral neck fracture (left)	Total hip replacement (left hip)
18	Female	NR	Femoral neck fracture (left)	NR

NR, no recording.

Cells used to explore the role of miR-22-5p in bone erosion were divided into the following four groups: i) mimics NC group (UHMWPE-treated hFOB cells transfected with NC miR-22-5p mimic, 100 pmol per 6 well plates); ii) mimics group (UHMWPE-treated hFOB cells transfected with miR-22-5p mimic, 100 pmol per 6 well plates); iii) inhibitor NC group (UHMWPE-treated hFOB cells transfected with a NC miR-22-5p inhibitor, 100 pmol per 6 well plates); and iv) inhibitor group (UHMWPE-treated hFOB cells transfected with a miR-22-5p inhibitor, 100 pmol per 6 well plates).

Cells used to detect interactions which occurred between MALAT1 and miR-22-5p were divided into the following four groups: i) blank group (UHMWPE-treated hFOB cells); ii) NC group (UHMWPE-treated hFOB cells transfected with pcDNA vector, 3 μg per 6 well plates); iii) mimics group (UHMWPE-treated hFOB cells transfected with miR-22-5p mimic, 3 μg per 6 well plates); and iv) MALAT1 + mimics group (UHMWPE-treated hFOB cells transfected with miR-22-5p mimic, 3 μg per 6 well plates, and pcDNA-MALAT1 vector, 2 μg per 6 well plates).

Cells used to detect whether VEGF intervention could recapitulate the effects of miR-22-5p overexpression were divided into the following three groups: i) blank group (UHMWPE-treated hFOB cells); ii) NC group (UHMWPE-treated hFOB cells transfected with NC siRNA, 100 pmol per 6 well plates); and iii) siVEGF group (UHMWPE-treated hFOB cells transfected with specific VEGF siRNA, 100 pmol per 6 well plates).

Reverse transcription-quantitative polymerase chain reaction (RT-qPCR). Total RNA was extracted from different clinical tissue and cell samples using an RNA Purified Total RNA Extraction kit according to the manufacturer's instructions (cat. no. RP1201; BioTeke Corporation, Beijing, China). GAPDH was selected as the reference gene. cDNA templates were constructed by reverse transcription of RNA using Super M-MLV reverse transcriptase (cat. no. PR6502; BioTeke Corporation). The mixture was incubated at 70˚C for 5 min and then incubated at 37˚C for 5 min. Each 20 μl reaction mixture contained 10 μl of SYBR Premix Ex Taq II (Clontech Laboratories, Inc., Mountainview, CA, USA) and 0.5 μl of each primer. RT-qPCR was performed as follows: pre-denaturation at 95˚C for 10 sec, followed by 40 cycles of denaturation at 95˚C for 10 sec and elongation at 60˚C for 30 sec. Relative expression levels were calculated using DataAssist software, version 3.0 (Applied Biosystems; Thermo Fisher Scientific, Inc., Waltham, MA, USA), and the formula: $2^{-[Cq(Gene) - Cq(GAPDH)]}$. Each assay was performed three times. The primers used in this study are presented in Table II.

Western blot analyses. The total proteins from different samples were extracted using a Total Protein Extraction kit according to the manufacturer's instructions (cat. no. WLA019; Wanleibo Co., Ltd., Beijing, China). GAPDH was used as an internal reference protein. The protein concentration of each sample was determined using the bicinchoninic acid method. An aliquot of protein (40 μg) from each sample subjected to 10% SDS-PAGE performed at 80 V for 2.5 h. The separated proteins were transferred onto polyvinylidene difluoride membranes, which were then washed with TBS-Tween for 5 min, and subsequently incubated with a powdered skim milk solution for 1 h. Subsequently, the membranes were incubated with primary antibodies against OPG (1:1,000), RANKL (1:500), VEGF (1:500) or GAPDH (1:500) at 4˚C overnight. Following incubation, the membranes were washed four more times with TBS-Tween, and then incubated with secondary

Table II. Primer sequences used in quantitative polymerase chain reaction.

Genes	Sequences (5'-3')
OPG	F: GCTGCTCAGTTTGTGGCG
	R: TGGACCTGGTTACCTATCATTTCT
RANK	F: CATGTTTACTTGCCCGGTTTA
	R: AGCTGTGAGTGCTTTCCCTTT
RANKL	F: TGCCAACATTTGCTTTCG
	R: TTCCTCCTTTCATCAGGGTAT
MALAT1	F: GCAGGGAGAATTGCGTCATT
	R: TTCTTCGCCTTCCCGTACTT
VEGF	F: TGTGTATACTCGCGCTACCT
	R: GATCTGCATCCGGACTTGGT
miR-22-5p	F: CTCAACTGGTGTCGTGGAGTCGG CAATTCAGTTGAGTCAAGAA
	R: TACACTCCAGCTGGGATTTCG AACGGTGACT
U6	F: CTCGCTTCGGCAGCACA
	R: AACGCTTCACGAATTTGCGT
β-actin	F: ATCGTGCGTGACATTAAGGAGAAG
	R: AGGAAGGAAGGCTGGAAGAGTG

F, forward; R, reverse; OPG, osteoprotegerin; RANK, receptor activator of nuclear factor-κB ligand; RANKL, RANK ligand; MALAT1, metastasis-associated lung adenocarcinoma transcript 1; VEGF, vascular endothelial growth factor; miR, microRNA.

IgG-horseradish peroxidase antibodies [1:5,000; goat anti-mouse IgG (BA1050) and goat anti-rabbit IgG (BA1054), Wuhan Boster Biological Technology, Ltd.] for 45 min at 37˚C. Following incubation, the membranes were washed six times with TBS-Tween, and the blots were developed using Beyo ECL Plus reagent (Thermo Fisher Scientific, Inc.). The images were recorded using a gel imaging system.

Cell Counting Kit-8 assay (CCK-8). CCK-8 assays were performed to detect cell proliferation. Approximately $1x10^4$ hFOB cells were seeded into each well of a 96-well plate and cultured for 72 h. The numbers of viable cells were determined using CCK-8 (Dojindo Molecular Technologies, Inc., Kumamoto, Japan) at 0, 24, 48, and 72 h after seeding. Briefly, after treatment with CCK-8 at 37˚C for 1 h, the absorbance of the hFOB cells at 450 nm was measured using a microplate reader (Rayto Life and Analytical Sciences Co., Ltd., München, Germany).

Cell viability assay. Cell viability further assessed using the 5-ethynyl-2'-deoxyuridine (EdU) assay as performed with a Cell-Light™ EdU kit (Guangzhou RiboBio Co., Ltd., Guangzhou, China). The viability of cells subjected to different treatments was assessed using a flow cytometer (Accuri C6; BD Biosciences, Franklin Lakes, NJ, USA) as described below.

Flow cytometry. The percentage of apoptotic cells in each sample was determined by using flow cytometry in conjunction with an Annexin V-FITC/PI Apoptosis Detection kit (cat. no. BB-4101-2; BestBio Co., Shanghai, China; http://www.beibokit.com/goods.php?id=53) as described in instructions provided by the manufacturer. Briefly, cultured cells from different time-points were incubated with 5 μl Annexin V for 10 min at room temperature, and then resuspended in binding buffer supplemented with 5 μl propidium iodide. The percentage of apoptotic cells was determined by flow cytometry. Following staining, the cells were gated into quadrants, and the rate of apoptosis was calculated as follows: Upper right (UR) quadrant + lower right (LR) quadrant indicated the percentage of apoptotic cells, which equaled the sum of the late apoptotic rate (UR) and the early apoptotic rate (LR).

miRNA targets mRNA prediction. Targets mRNA of miRNA were identified using the following websites: microRNA.org and targetscan.org.

Dual luciferase assay. The concentration of hFOB cells was adjusted to $1x10^4$ cells/ml, and the cells were then incubated for 24 h prior to co-transfection with different combinations of vectors.

Cells used to determine interactions between VEGF and miR-22-5p were divided into the following four groups: i) WT + NC group (cells were co-transfected with WT VEGF plasmid, 0.2 μg, and NC miR-22-5p mimics, 5 pmol); ii) WT + mimics group (cells were co-transfected with WT VEGF plasmid, 0.2 μg, and miR-22-5p mimics, 5 pmol); iii) MUT + NC group (cells were co-transfected with MUT VEGF plasmid, 0.2 μg, and NC miR-22-5p mimics, 5 pmol); iv) MUT + mimics group (cells were co-transfected with MUT VEGF plasmid, 0.2 μg, and miR-22-5p mimics, 5 pmol). Following transfection, the luciferase activity was measured using the Dual-Luciferase Reporter Assay kit (cat. no. E1910; Promega Corporation). Results were normalized to Renilla luciferase activity. The same method of grouping cells was used when assessing interactions between MATAL1 and miR-22-5p.

Statistical analysis. All data are expressed as the mean ± standard deviation. Student's t-test, analysis of variance, and Duncan's post hoc multiple comparisons test were performed using GraphPad Prism 6 software (GraphPad Software, Inc., San Diego, CA, USA). $P \leq 0.05$ was considered to indicate a statistically significant difference.

Results

MALAT1 expression in upregulated in samples with bone erosion. The expression of MALAT1 and molecules associated with skeletal development was comprehensively investigated in clinical samples. Demographic and clinical characteristics of the patients that donated the samples are presented in Table I. The RANKL/RANK/OPG system is considered as an important signal transduction pathway in osteolysis. We found that the expression of RANK was lower in loose tissue samples comparing with normal synovial tissues (Fig. 1). By contrast, molecules that promote osteolysis showed significantly enhanced levels of expression (Fig. 1) in samples of loose tissue compared with normal control samples. Furthermore, MALAT1 RNA levels were higher in loose samples compared with normal samples.

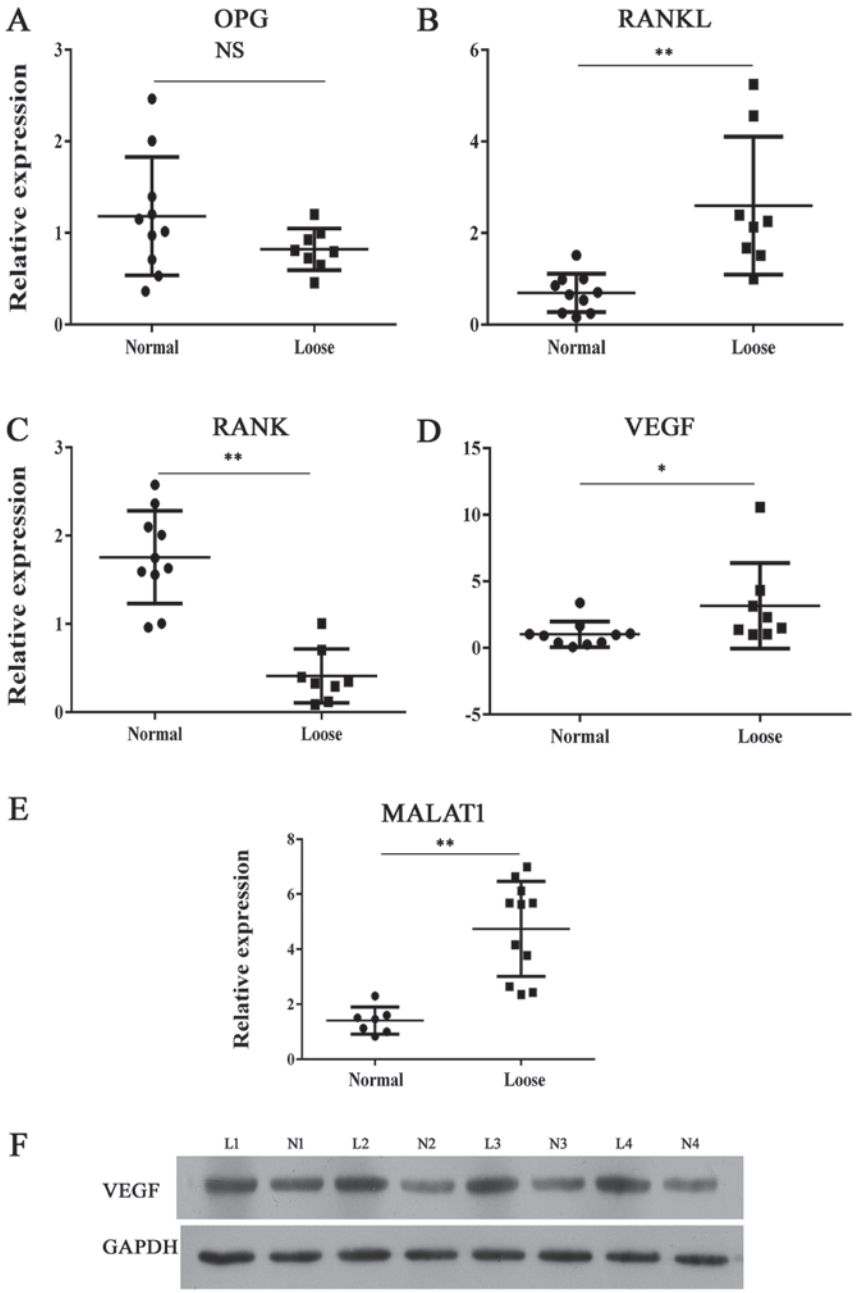

Figure 1. Expression of bone metabolism indicators and MALAT1. Reverse transcription-quantitative polymerase chain reaction analysis of (A) OPG, (B) RANKL, (C) RANK, (D) VEGF and (E) MALAT1 expression in clinical interface membrane tissues and normal tissues. (F) Representative images from western blot analysis of VEGF protein expression in interface membrane tissues showed enhanced expression of VEGF. *P<0.05, **P<0.01 vs. normal sample. OPG, osteoprotegerin; NS, not significant; RANK, receptor activator of nuclear factor-κB; RANKL, RANK ligand; MALAT1, metastasis-associated lung adenocarcinoma transcript 1; VEGF, vascular endothelial growth factor; L, loose; N, normal.

Knockdown of MALAT1 decreases cell viability and induces cell apoptosis in hFOB 1.19 cells. The human hFOB 1.19 fetal osteoblastic cell line has been used as an *in vitro* osteolysis model in numerous studies. Thus, in the present study, MALAT1 gene expression was altered in the cell line to assess its role in the osteolytic process. Following silencing the MALAT1 gene using siRNA, the viability of UHMWPE-treated hFOB 1.19 cells was significantly reduced compared with the NC siRNA group (Fig. 2A and B). Results of CCK-8 assays indicated that the MALAT1 knockdown UHMWPE-treated hFOB 1.19 cells were significantly less viable than UHMWPE-treated hFOB 1.19 cells from 48 h of the assay (Fig. 2A). These results were further validated in the EdU assay, in which the numbers of EdU-positive cells was reduced in the siMALAT1 group compared with the NC group (Fig. 2B). Furthermore, the percentage of apoptotic cells in the siMALAT1 group increased compared with the NC group, in conjunction with their decreased viability (Fig. 2C), indicating that MALAT1 knockdown decreased the survival rates of UHMWPE-treated hFOB 1.19 cells. At the molecular level, knockdown of MALAT1 reduced the protein expression levels of RANKL and VEGF, and enhanced the levels of OPG (Fig. 2D).

Knockdown of VEGF recapitulated the biological effects observed following miR-22-5p overexpression. To further

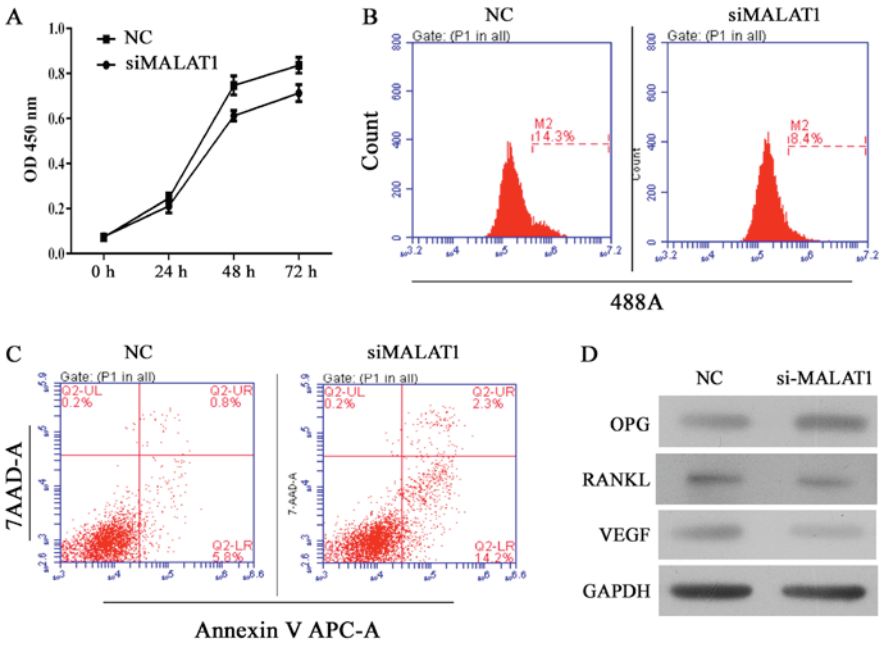

Figure 2. Knockdown of MALAT1 inhibits cell growth and induces apoptosis in ultra-high molecular weight polyethylene-treated hFOB 1.19 cells, and the effect was associated is upregulation of OPG, and downregulation of RANKL and VEGF. (A) Quantitative analysis of CCK-8 assay results at 24, 48 and 72 h after siRNA transfection. (B) Representative images of 5-ethynyl-2'-deoxyuridine assay results after 48 h of siRNA transfection. (C) Representative images of apoptosis rates as detected by flow cytometry after 48 h of siRNA transfection. (D) Representative images from western blot analyses of OPG, RANKL and VEGF protein expression after 48 h of siRNA transfection. All experiments were repeated at least 3 times. OD, optical density; NC, negative control; si, small interfering RNA; MALAT1, metastasis-associated lung adenocarcinoma transcript 1; 7-AAD, 7-aminoactinomycin D; APC, allophycocyanin; OPG, osteoprotegerin; RANKL, receptor activator of nuclear factor-κB ligand; VEGF, vascular endothelial growth factor.

corroborate the pathway of miR-22-5p targeting VEGF, which in turn regulated RANKL and OPG, UHMWPE-treated hFOB 1.19 cells were treated with siVEGF to determine whether this intervention induces the same effects as miR-22-5p over-expression. The EdU and CCK-8 assays demonstrated that the viability of UHMWPE-treated hFOB 1.19 cells was decreased by siVEGF transfection (Fig. 3A and B). Furthermore, the apoptosis of UHMWPE-treated hFOB 1.19 cells was induced by siVEGF (Fig. 3D). Western blot results (Fig. 3C) demonstrated that inhibited VEGF expression increased OPG expression, while RANKL was decreased in hFOB 1.19 cells. These results indicated that knockdown of VEGF induces the same biological effects observed following miR-22-5p over-expression.

miR-22-5p decreases cell viability and induces apoptosis in hFOB 1.19 cells, and reduces VEGF expression. Expression of miR-22-5p was investigated in clinical samples of abnormal bone tissue. As demonstrated in Fig. 4A, bone erosion was associated with decreased miR-22-5p production; thus, the role of miR-22-5p in osteolysis was examined further. VEGF was demonstrated to be a direct target of miR-22-5p and this conclusion was validated in a dual luciferase assay, in which transfection of miR-22-5p inhibited luciferase activity from the plasmid containing the 3'UTR of VEGF (Fig. 4B and C). Subsequently, UHMWPE-treated hFOB 1.19 cells were transfected with mimics or an inhibitor of miR-22-5p. The viability of UHMWPE-treated hFOB 1.19 cells was decreased by miR-22-5p mimics and miR-22-5p inhibitor (Fig. 5A and B). Western blot analysis demonstrated that the effect of miR-22-5p on the viability of UHMWPE-treated hFOB 1.19 cells was associated changes in the levels of OPG, RANKL and VEGF expression. Consistent with results of the dual luciferase assay, miR-22-5p mimics reduced VEGF protein expression (Fig. 5C). Furthermore, the expression of RANKL, which is reported to function in conjunction with VEGF during osteoclast differentiation (25), was also reduced by miR-22-5p mimics (Fig. 5C). In contrast to the effects on VEGF and RANKL, expression of the anti-osteolysis factor OPG was induced by miR-22-5p mimics and suppressed by miR-22-5p inhibitors (Fig. 5C). Furthermore, apoptosis of UHMWPE-treated hFOB 1.19 cells was induced by miR-22-5p mimics and suppressed by an miR-22-5p inhibitor (Fig. 5D). These results demonstrated that in contrast to the effect of MALAT1, miR-22-5p inhibited the osteolytic process.

MALAT1 induces osteolysis by upregulating the expression of VEGF and RANKL. MALAT1 was expressed at relatively high levels in samples of loose interface membrane tissue compared with normal samples (Fig. 1E). As Demonstrated in Fig. 6A and B, miR-22-5p targets MALAT1 due to its matched sequence and interaction between MALAT1 and miR-22-5p was validated in a dual luciferase assay. To further examine the modulating sequence of the two RNA members, hFOB 1.19 cells were transfected with different combinations of MALAT1 expression vector and miR-22-5p mimics. It was observed that when co-transfected, the pro-survival effect of MALAT1 on hFOB 1.19 cells reduced the anti-survival effect of miR-22-5p. Furthermore, when tested in the EdU and CCK-8 assays, cells transfected with pcDNA-MALAT1 and miR-22-5p mimics exhibited increased viability compared with cells transfected with miR-22-5p mimics (Fig. 7A and B).

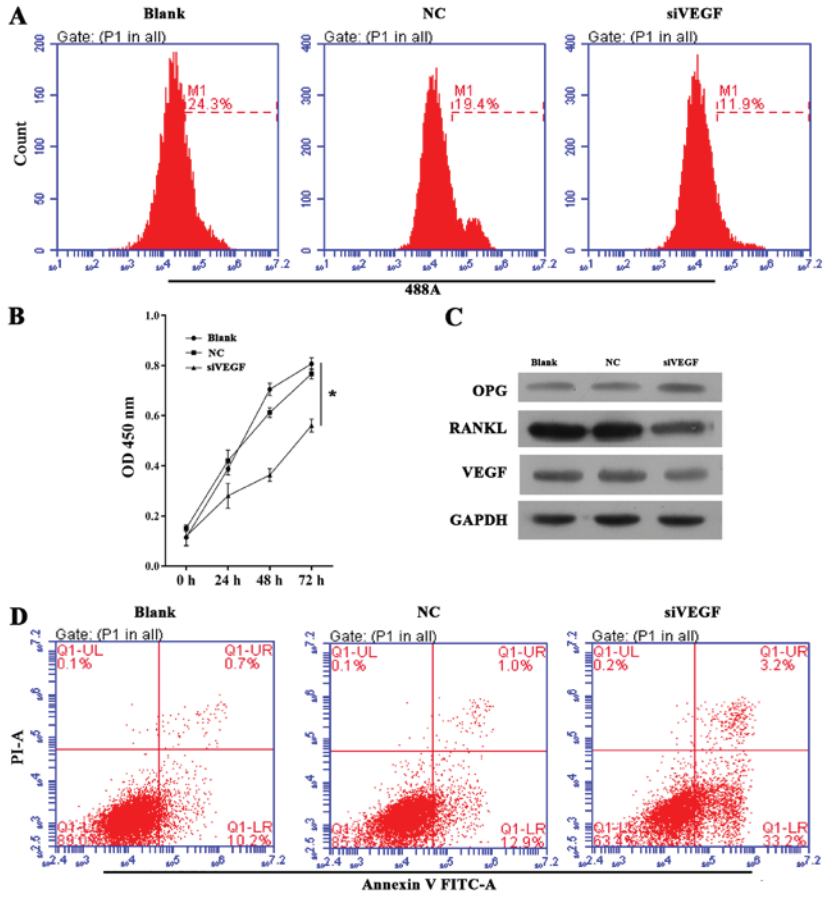

Figure 3. Effect of VEGF knockdown on cell growth, apoptosis and OPG, RANKL and VEGF expression in ultra-high molecular weight polyethylene-treated hFOB 1.19 cells. (A) Representative images from 5-ethynyl-2'-deoxyuridine assays after 48 h of siRNA transfection. (B) Quantitative analysis of results of CCK-8 assays at 24, 48 and 72 h after siRNA transfection. (C) Representative images from western blot analyses of OPG, RANKL and VEGF expression after 48 h of siRNA transfection. (D) Representative images showing apoptosis rates detected by flow cytometry after 48 h of siRNA transfection. All experiments were repeated at least 3 times. NC, negative control; si, small interfering RNA; VEGF, vascular endothelial growth factor; OD, optical density; OPG, osteoprotegerin; RANKL, receptor activator of nuclear factor-κB ligand; PI, propidium iodide; FITC, fluorescein isothiocyanate.

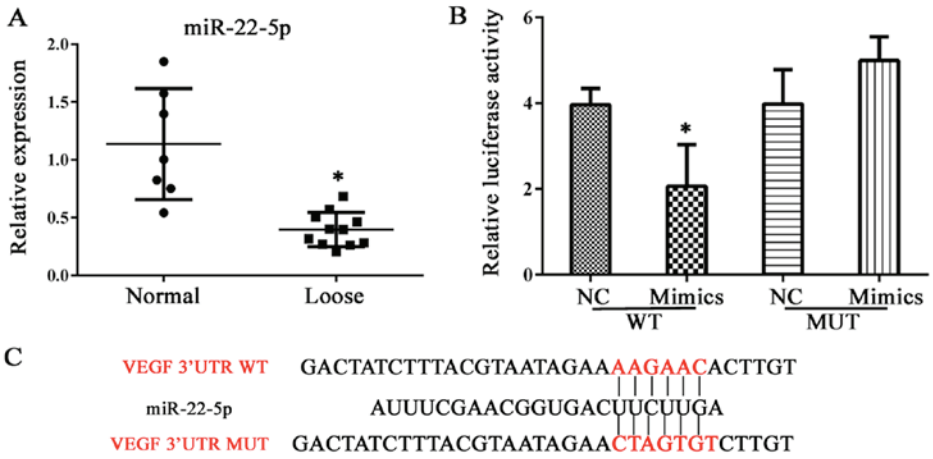

Figure 4. miR-22-5p expression is reduced in interface membrane tissue and VEGF is a direct target of miR-22-5p. (A) Reverse transcription-quantitative polymerase chain reaction analysis of miR-22-5p expression in interface membrane tissues (n=7-11). (B) Dual luciferase assay results indicating that interaction occurs between VEGF and miR-22-5p. The relative luciferase activity was examined at 48 h after transfection. The experiments was repeated at least 3 times. (C) Sequence alignment of miR-22-5p and the 3'UTR of VEGF as analyzed using TargetScan and an miRDB algorithm. miR, microRNA; NC, negative control; WT wild type; MUT, mutated; VEGF, vascular endothelial growth factor; UTR, untranslated region.

The antagonistic effect of MATAL1 reversed the decreased levels of RANKL and VEGF expression induced by miR-22-5p mimics (Fig. 7C). The above results indicate that MALAT1 induces osteolysis, potentially by inhibiting miR-22-5p expression, and thus further initiating pro-osteolysis signaling processes.

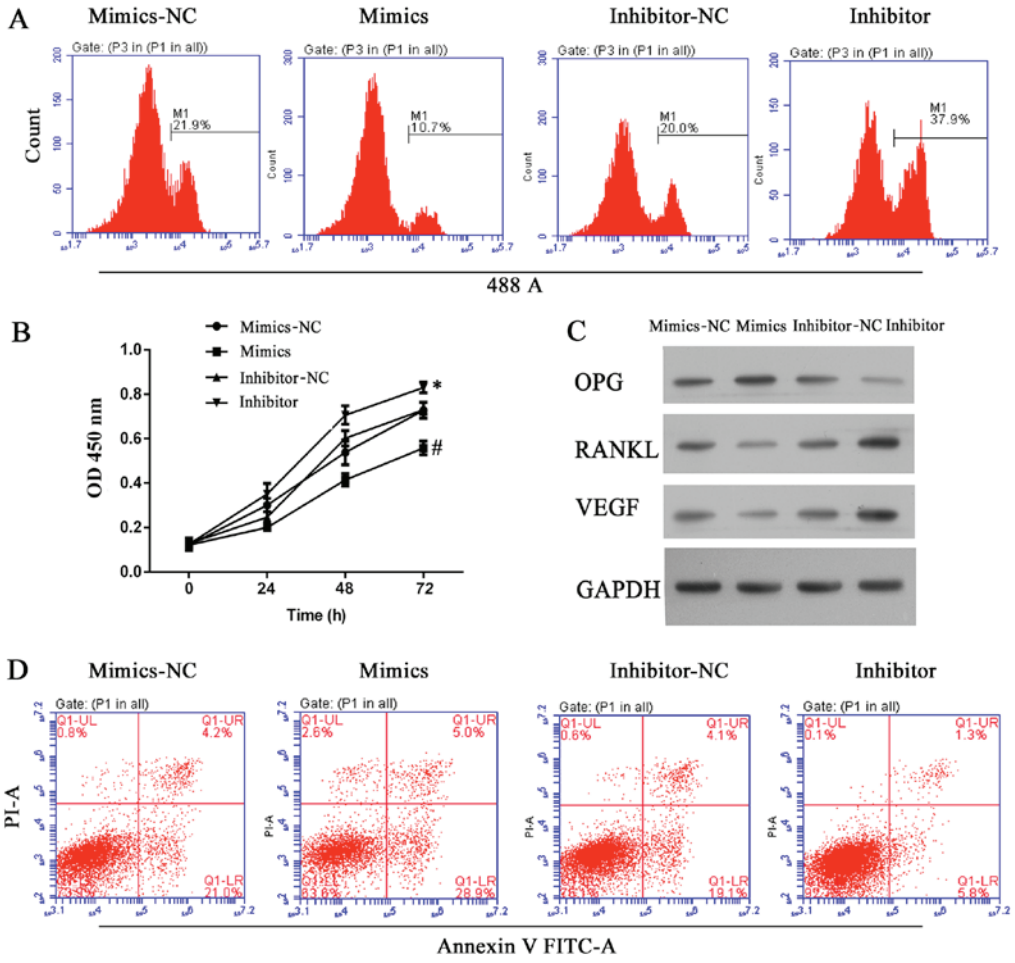

Figure 5. miR-22-5p antagonized osteolysis by inhibiting cell growth and inducing apoptosis in ultra-high molecular weight polyethylene-treated hFOB 1.19 cells, and the effect was associated with upregulation of OPG and downregulation of RANKL and VEGF. (A) Representative images from 5-ethynyl-2'-deoxyuridine assays after 48 h of transfection. (B) Quantitative analysis of results from CCK-8 assays at 24, 48 and 72 h after transfection. (C) Representative images from western blot analyses of OPG, RANKL and VEGF expression after 48 h of transfection. (D) Representative images showing apoptosis rates as detected by flow cytometry at 48 h after transfection. All experiments were repeated at least 3 times. NC, negative control; OD, optical density; OPG, osteoprotegerin; RANKL, RANKL, receptor activator of nuclear factor-κB ligand; VEGF, vascular endothelial growth factor; PI, propidium iodide; FITC, fluorescein isothiocyanate.

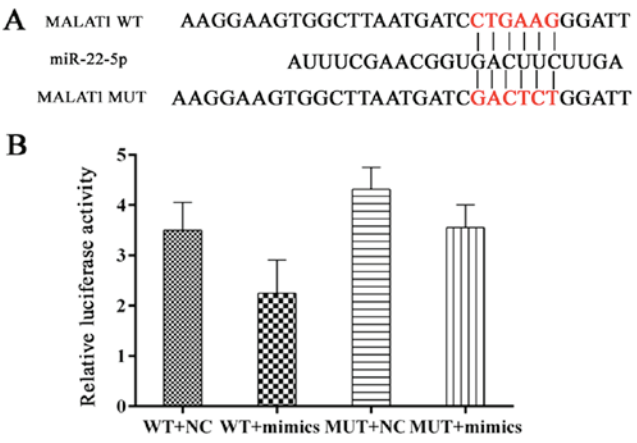

Figure 6. MALAT1 directly interacts with miR-22-5p. (A) Sequence alignment of miR-22-5p and MALAT1. (B) Quantitative analysis from the dual luciferase assay indicated that there is interaction between MALAT1 and miR-22-5p. The relative luciferase activity was examined at 48 h after transfection. The experiments was repeated at least 3 times. MALAT1, metastasis-associated lung adenocarcinoma transcript 1; WT, wild type; NC, negative control; MUT, mutated; miR, microRNA.

Discussion

Homeostasis of bone metabolism depends on maintaining a balance between osteoblastic bone formation and osteoclastic bone resorption (22). It is commonly recognized that the transition between osteoblastic and osteoclastic processes is regulated by the relative levels of OPG and RANKL (26,27). Therefore, upstream regulators of these two indicators assist in modulating bone metabolism, and represent potential targets for treating bone erosion associated with an implanted prosthesis. In the present study, MALAT1 lncRNA induced the osteoclastic process in UHMWPE-treated hFOB 1.19 cells by suppressing miR-22-5p activity. This suppression may inhibit osteolysis by blocking VEGF signaling and increasing RANKL activity.

MALAT1 is a typical member of the lncRNA family, which is a novel class of mRNA-like transcripts that have numerous structural and functional roles cells. Previous studies have reported that overexpression of MALAT1 modulates alternative splicing, and is associated with metastasis and a poor prognosis in patients with lung cancer (28,29). Furthermore, a deficiency

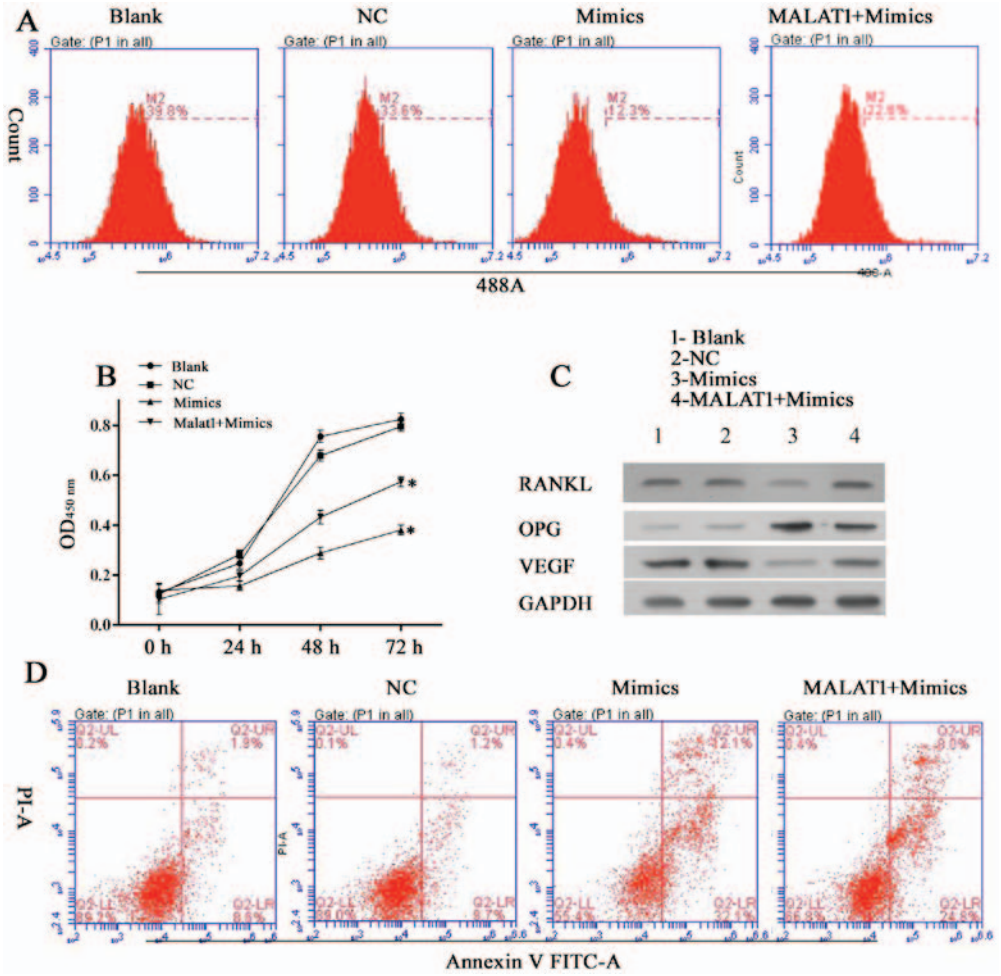

Figure 7. MALAT1 induces osteolysis by suppressing miR-22-5p activity. (A) Representative images of 5-ethynyl-2'-deoxyuridine assay results at 48 h after transfection. (B) Quantitative analysis of results from CCK-8 assays at 48 h after transfection. (C) Representative images from western blot analyses of OPG, RANKL and VEGF expression at 48 h after transfection. (D) Representative images showing apoptosis rates as detected by flow cytometry at 48 h after transfection. All experiments were repeated at least 3 times. NC, negative control; MALAT1, metastasis-associated lung adenocarcinoma transcript 1; OD, optical density; RANKL, receptor activator of nuclear factor-κB ligand; OPG, osteoprotegerin; VEGF, vascular endothelial growth factor; PI, propidium iodide; FITC, fluorescein isothiocyanate.

of MALAT1 led to enhanced sprouting and migration of endothelial cells in a sphere model (30). Che *et al* (22) reported that MALAT1 knockdown reversed RANKL-induced cell growth inhibition and cell cycle arrest in normal hFOB 1.19 cells. Additionally, the previous study also demonstrated that MALAT1 knockdown by siRNA significantly downregulated the levels of OPG protein in hFOB 1.19 cells, suggesting the modulation of OPG by MALAT1 in osteoblastic cells (22). In the present study, it was initially validated that MALAT1 was overexpressed in clinical samples, and overexpression was associated with a downregulation of OPG and upregulation of RANKL. In healthy bone tissue, OPG acts as a soluble receptor antagonist that neutralizes RANKL, and thus blocks RANKL-RANK interaction. This blocking effect maintains a balance between osteoblastic and osteoclastic metabolic processes (26,31,32). To further determine the role of MALAT1 in osteolysis, hFOB 1.19 cells were pre-treated with UHMWPE, which induced the osteoclastic process in those cells. The cells were then transfected with MALAT1 specific siRNA, and cell growth was inhibited by MALAT1 knockdown. Furthermore, the decrease in cell growth was accompanied by increased OPG expression, and suppression of RANKL and VEGF expression. UHMWPE-treated hFOB 1.19 cells were characterized by osteoclastic features; therefore, the inhibitory effect of MALAT1 knockdown on the osteoclastic process in those cells confirmed that MALAT1 has a role in the onset of osteolysis. Accordingly, MALAT1 exerted its function via the OPG/RANKL pathway. It was also demonstrated that other molecules have crucial roles in bone metabolism, as VEGF expression (33-35) was also modulated by MALAT1 knockdown.

Results of previous studies suggest that the potential connection between MALAT1 and VEGF may be modulated by two separate pathways. Yamakuchi *et al* (20) reported that VEGF protein expression was reduced in cells that overexpressed miR-22 (20), and Tang *et al* (23) reported that MALAT1 protects the endothelium from oxidized low-density lipoprotein-induced endothelial dysfunction by competing with miR-22 (23). Those findings justified performing a comprehensive investigation of the regulating sequence among those three molecules. In the present study, a dual luciferase assay was used to validate that VEGF and MALAT1 directly interact with miR-22-5p. Transfection with miR-22-5p inhibited the growth of UHMWPE-treated hFOB 1.19 cells, and reduced VEGF expression. However, it was also found that overexpression of MALAT1 in UHMWPE-treated

hFOB 1.19 cells reversed the inhibiting effect of miR-22-5p mimics on the cells, and increased VEGF protein levels. The potential regulatory effect of MALAT1 on miR-22-5p can be explained by 'competitive endogenous RNA (ceRNA)' theory. That theory suggests that miRNAs function as gene-regulating non-coding RNAs by directing the RNA-induced silencing complex towards miRNA-response elements (MREs) (36,37). These MREs are located on the 3'UTR, coding sequence and 5'UTR of mRNA, or non-protein coding transcripts such as lncRNAs (38). The vast majority of RNA molecules harbor several MREs, and are thus repressed by different miRNAs. This target multiplicity underlies the hypothesis that different RNAs (either pseudo-targets or legitimate targets) compete for limited pools of miRNAs (39,40), and thus act as ceRNAs. This suggests that any regulatory effect of MALAT1 on VEGF may be due to inhibition of miR-22-5p, and further supports the notion that MALAT1 induces osteolysis. In addition to the MALAT1/miR-22-5p mechanism for regulating VEGF, MALAT1 may also induce VEGF activity via a RANKL-dependent mechanism. Zhang *et al* (41) reported that VEGF-C is a target gene of RANKL, and that VEGF-C expression was upregulated by RANKL in osteoclasts (41). Although such a mechanism was not explicitly validated in the present study, the suppressed VEGF levels found after MALAT1 knockdown may partially reflect participation of a MALAT1/RANKL/VEGF pathway in the initiation of osteolysis.

In conclusion, the findings of the current study demonstrate that MALAT1 has a key role in the onset of osteolysis. MALAT1 was upregulated in interface membrane samples from patients receiving a knee replacement operation compared with normal controls. Furthermore, knockdown of MALAT1 inhibited the growth of UHMWPE-treated hFOB 1.19 cells. The promoting effect of MALAT1 on the osteoclastic process was exerted via three pathways: i) MALAT1 initiated RANKL signaling by decreasing the OPG level; ii) MALAT1 increased VEGF levels via a mechanism that inhibited miR-22-5p; and iii) MALAT1 increased VEGF levels in a RANKL-dependent manner. Thus, MALAT1 is a potential target for treating osteolysis associated with an implanted prosthesis. However, additional comprehensive studies are required prior to developing treatment strategies based on MALAT1.

Acknowledgements

This study was supported by the Fundamental Research Funds for Central Universities (grant no. 2012QNZT119) and the National Natural Science Foundation of China (grant no. 8170090962).

Competing interests

The authors declare that they have no competing interests.

References

1. Kandahari AM, Yang X, Laroche KA, Dighe AS, Pan D and Cui Q: A review of UHMWPE wear-induced osteolysis: the role for early detection of the immune response. Bone Res 4: 16014, 2016.
2. Harris WH: Wear and periprosthetic osteolysis: the problem. Clin Orthop Relat Res 393: 66-70, 2001.
3. Fu C, Xie J, Hu N, Liang X, Chen R, Wang C, Chen C, Xu C, Huang W and Paul Sung KL: Titanium particles up-regulate the activity of matrix metalloproteinase-2 in human synovial cells. Int Orthop 38: 1091-1098, 2014.
4. Katsuyama E, Miyamoto H, Kobayashi T, Sato Y, Hao W, Kanagawa H, Fujie A, Tando T, Watanabe R, Morita M, *et al*: Interleukin-1 receptor-associated kinase-4 (IRAK4) promotes inflammatory osteolysis by activating osteoclasts and inhibiting formation of foreign body giant cells. J Biol Chem 290: 716-726, 2015.
5. Vallés G, Pérez C, Boré A, Martín-Saavedra F, Saldaña L and Vilaboa N: Simvastatin prevents the induction of interleukin-6 gene expression by titanium particles in human osteoblastic cells. Acta Biomater 9: 4916-4925, 2013.
6. Beck RT, Illingworth KD and Saleh KJ: Review of periprosthetic osteolysis in total joint arthroplasty: an emphasis on host factors and future directions. J Orthop Res 30: 541-546, 2012.
7. Wooley PH and Schwarz EM: Aseptic loosening. Gene Ther 11: 402-407, 2004.
8. Jiang Y, Jia T, Wooley PH and Yang SY: Current research in the pathogenesis of aseptic implant loosening associated with particulate wear debris. Acta Orthop Belg 79: 1-9, 2013.
9. Nakagawa M, Kaneda T, Arakawa T, Morita S, Sato T, Yomada T, Hanada K, Kumegawa M and Hakeda Y: Vascular endothelial growth factor (VEGF) directly enhances osteoclastic bone resorption and survival of mature osteoclasts. FEBS Lett 473: 161-164, 2000.
10. Favus MJ: Primer on the Metabolic Bone Diseases and Disorders of Mineral Metabolism. Rittenhouse Book Distributors, 2006.
11. Leung DW, Cachianes G, Kuang WJ, Goeddel DV and Ferrara N: Vascular endothelial growth factor is a secreted angiogenic mitogen. Science 246: 1306-1309, 1989.
12. Goad DL, Rubin J, Wang H, Tashjian AH Jr and Patterson C: Enhanced expression of vascular endothelial growth factor in human SaOS-2 osteoblast-like cells and murine osteoblasts induced by insulin-like growth factor I. Endocrinology 137: 2262-2268, 1996.
13. Gerber HP, Vu TH, Ryan AM, Kowalski J, Werb Z and Ferrara N: VEGF couples hypertrophic cartilage remodeling, ossification and angiogenesis during endochondral bone formation. Nat Med 5: 623-628, 1999.
14. Henriksen K, Karsdal M, Delaisse JM and Engsig MT: RANKL and vascular endothelial growth factor (VEGF) induce osteoclast chemotaxis through an ERK1/2-dependent mechanism. J Biol Chem 278: 48745-48753, 2003.
15. Gibb EA, Vucic EA, Enfield KS, Stewart GL, Lonergan KM, Kennett JY, Becker-Santos DD, MacAulay CE, Lam S, Brown CJ, *et al*: Human cancer long non-coding RNA transcriptomes. PLoS One 6: e25915, 2011.
16. Gutschner T and Diederichs S: The hallmarks of cancer: a long non-coding RNA point of view. RNA Biol 9: 703-719, 2012.
17. Liu B, Peng XC, Zheng XL, Wang J and Qin YW: miR-126 restoration down-regulate VEGF and inhibit the growth of lung cancer cell lines in vitro and in vivo. Lung Cancer 66: 169-175, 2009.
18. Cascio S, D'Andrea A, Ferla R, Surmacz E, Gulotta E, Amodeo V, Bazan V, Gebbia N and Russo A: miR-20b modulates VEGF expression by targeting HIF-1 alpha and STAT3 in MCF-7 breast cancer cells. J Cell Physiol 224: 242-249, 2010.
19. Lei Z, Li B, Yang Z, Fang H, Zhang GM, Feng ZH and Huang B: Regulation of HIF-1alpha and VEGF by miR-20b tunes tumor cells to adapt to the alteration of oxygen concentration. PLoS One 4: e7629, 2009.
20. Yamakuchi M, Yagi S, Ito T and Lowenstein CJ: MicroRNA-22 regulates hypoxia signaling in colon cancer cells. PLoS One 6: e20291, 2011.
21. Huang S, Wang S, Bian C, Yang Z, Zhou H, Zeng Y, Li H, Han Q and Zhao RC: Upregulation of miR-22 promotes osteogenic differentiation and inhibits adipogenic differentiation of human adipose tissue-derived mesenchymal stem cells by repressing HDAC6 protein expression. Stem Cells Dev 21: 2531-2540, 2012.
22. Che W, Dong Y and Quan HB: RANKL inhibits cell proliferation by regulating MALAT1 expression in a human osteoblastic cell line hFOB 1.19. Cell Mol Biol 61: 7-14, 2015.
23. Tang Y, Jin X, Xiang Y, Chen Y, Shen CX, Zhang YC and Li YG: The lncRNA MALAT1 protects the endothelium against ox-LDL-induced dysfunction via upregulating the expression of the miR-22-3p target genes CXCR2 and AKT. FEBS Lett 589: 3189-3196, 2015.

24. Kauther MD, Xu J and Wedemeyer C: Alpha-calcitonin gene-related peptide can reverse the catabolic influence of UHMWPE particles on RANKL expression in primary human osteoblasts. Int J Biol Sci 6: 525-536, 2010.
25. Yao S, Liu D, Pan F and Wise GE: Effect of vascular endothelial growth factor on RANK gene expression in osteoclast precursors and on osteoclastogenesis. Arch Oral Biol 51: 596-602, 2006.
26. Lacey DL, Timms E, Tan HL, Kelley MJ, Dunstan CR, Burgess T, Elliott R, Colombero A, Elliott G, Scully S, *et al*: Osteoprotegerin ligand is a cytokine that regulates osteoclast differentiation and activation. Cell 93: 165-176, 1998.
27. Simonet WS, Lacey DL, Dunstan CR, Kelley M, Chang MS, Lüthy R, Nguyen HQ, Wooden S, Bennett L, Boone T, *et al*: Osteoprotegerin: a novel secreted protein involved in the regulation of bone density. Cell 89: 309-319, 1997.
28. Ji P, Diederichs S, Wang W, Böing S, Metzger R, Schneider PM, Tidow N, Brandt B, Buerger H, Bulk E, *et al*: MALAT-1, a novel noncoding RNA, and thymosin beta4 predict metastasis and survival in early-stage non-small cell lung cancer. Oncogene 22: 8031-8041, 2003.
29. Tripathi V, Ellis JD, Shen Z, Song DY, Pan Q, Watt AT, Freier SM, Bennett CF, Sharma A, Bubulya PA, *et al*: The nuclear-retained noncoding RNA MALAT1 regulates alternative splicing by modulating SR splicing factor phosphorylation. Mol Cell 39: 925-938, 2010.
30. Thum T and Fiedler J: LINCing MALAT1 and angiogenesis. Circ Res 114: 1366-1368, 2014.
31. Yasuda H, Shima N, Nakagawa N, Yamaguchi K, Kinosaki M, Mochizuki S, Tomoyasu A, Yano K, Goto M, Murakami A, *et al*: Osteoclast differentiation factor is a ligand for osteoprotegerin/osteoclastogenesis-inhibitory factor and is identical to TRANCE/RANKL. Proc Natl Acad Sci USA 95: 3597-3602, 1998.
32. Takahashi N, Udagawa N and Suda T: A new member of tumor necrosis factor ligand family, ODF/OPGL/TRANCE/RANKL, regulates osteoclast differentiation and function. Biochem Biophys Res Commun 256: 449-455, 1999.
33. Liu Y, Berendsen AD, Jia S, Lotinun S, Baron R, Ferrara N and Olsen BR: Intracellular VEGF regulates the balance between osteoblast and adipocyte differentiation. J Clin Invest 122: 3101-3113, 2012.
34. Hu K and Olsen BR: Osteoblast-derived VEGF regulates osteoblast differentiation and bone formation during bone repair. J Clin Invest 126: 509-526, 2016.
35. Tombran-Tink J and Barnstable CJ: Osteoblasts and osteoclasts express PEDF, VEGF-A isoforms, and VEGF receptors: possible mediators of angiogenesis and matrix remodeling in the bone. Biochem Biophys Res Commun 316: 573-579, 2004.
36. Guo H, Ingolia NT, Weissman JS and Bartel DP: Mammalian microRNAs predominantly act to decrease target mRNA levels. Nature 466: 835-840, 2010.
37. Hendrickson DG, Hogan DJ, McCullough HL, Myers JW, Herschlag D, Ferrell JE and Brown PO: Concordant regulation of translation and mRNA abundance for hundreds of targets of a human microRNA. PLoS Biol 7: e1000238, 2009.
38. Paraskevopoulou MD, Georgakilas G, Kostoulas N, Reczko M, Maragkakis M, Dalamagas TM and Hatzigeorgiou AG: DIANA-LncBase: experimentally verified and computationally predicted microRNA targets on long non-coding RNAs. Nucleic Acids Res 41: D239-D245, 2013.
39. Salmena L, Poliseno L, Tay Y, Kats L and Pandolfi PP: A ceRNA hypothesis: the Rosetta Stone of a hidden RNA language? Cell 146: 353-358, 2011.
40. Seitz H: Redefining microRNA targets. Curr Biol 19: 870-873, 2009.
41. Zhang Q, Guo R, Lu Y, Zhao L, Zhou Q, Schwarz EM, Huang J, Chen D, Jin ZG, Boyce BF, *et al*: VEGF-C, a lymphatic growth factor, is a RANKL target gene in osteoclasts that enhances osteoclastic bone resorption through an autocrine mechanism. J Biol Chem 283: 13491-13499, 2008.